JACS
JOURNAL OF THE AMERICAN CHEMICAL SOCIETY
Article
pubs.acs.org/JACS

New Pathways for Formation of Acids and Carbonyl Products in Low-Temperature Oxidation: The Korcek Decomposition of γ-Ketohydroperoxides

Amrit Jalan,[†] Ionut M. Alecu,[†,§] Rubén Meana-Pañeda,[‡] Jorge Aguilera-Iparraguirre,[†] Ke R. Yang,[‡] Shamel S. Merchant,[†] Donald G. Truhlar,*[,‡] and William H. Green*[,†]

[†]Department of Chemical Engineering, Massachusetts Institute of Technology, Cambridge, Massachusetts 02139, United States
[‡]Department of Chemistry, Supercomputing Institute, and Chemical Theory Center, University of Minnesota, Minneapolis, Minnesota 55455, United States

Supporting Information

ABSTRACT: We present new reaction pathways relevant to low-temperature oxidation in gaseous and condensed phases. The new pathways originate from γ-ketohydroperoxides (KHP), which are well-known products in low-temperature oxidation and are assumed to react only via homolytic O−O dissociation in existing kinetic models. Our *ab initio* calculations identify new exothermic reactions of KHP forming a cyclic peroxide isomer, which decomposes via novel concerted reactions into carbonyl and carboxylic acid products. Geometries and frequencies of all stationary points are obtained using the M06-2X/MG3S DFT model chemistry, and energies are refined using RCCSD(T)-F12a/cc-pVTZ-F12 single-point calculations. Thermal rate coefficients are computed using variational transition-state theory (VTST) calculations with multidimensional tunneling contributions based on small-curvature tunneling (SCT). These are combined with multistructural partition functions (Q^{MS-T}) to obtain direct dynamics multipath (MP-VTST/SCT) gas-phase rate coefficients. For comparison with liquid-phase measurements, solvent effects are included using continuum dielectric solvation models. The predicted rate coefficients are found to be in excellent agreement with experiment when due consideration is made for acid-catalyzed isomerization. This work provides theoretical confirmation of the 30-year-old hypothesis of Korcek and co-workers that KHPs are precursors to carboxylic acid formation, resolving an open problem in the kinetics of liquid-phase autoxidation. The significance of the new pathways in atmospheric chemistry, low-temperature combustion, and oxidation of biological lipids are discussed.

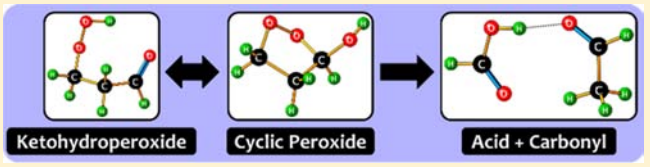

1. INTRODUCTION

Liquid-phase oxidation of hydrocarbons has been the subject of experimental and theoretical investigations for over 75 years, owing to its applications in many areas of practical importance.[1] Mechanistic modeling of the free radical chemistry of liquid-phase autoxidation also provides insight into low-temperature gas-phase ignition chemistry which is critical in modeling novel engine technologies like homogeneous charge compression ignition (HCCI).[2] Liquid-phase autoxidation is also the basis for understanding complex processes like lipid degradation in biological systems[3] and thermal stability of polymers and lubricants.[4]

Even though there have been many experimental studies on the oxidation of various liquid substrates (alkanes, ketones, alcohols, etc.),[5] very few report the time evolution of products because of difficulties in separation and analysis. Consequently, although the chemical identity of primary and secondary products like hydroperoxides, alcohols, acids, aldehydes, and ketones has been established, elementary reactions leading to their formation and consumption are known for only a few cases. Kinetic models published by Pfaendtner and Broadbelt[6] are representative of the current state of understanding of elementary reactions involved in these systems.

The experimental work of Korcek and co-workers[5a−d,7] on liquid hexadecane oxidation performed over 30 years ago provides the most detailed available analysis of both primary and secondary oxidation products. In addition to measuring the yields of monohydroperoxides (ROOH), they employed a complex analytical scheme (using three different reducing agents) and liquid chromatography techniques to distinguish and quantify the yields of other primary products like ketohydroperoxides (HOOQ′=O, KHP) and dihydroperoxides ($Q(OOH)_2$) which are formed in the early stages of oxidation and retain the original C_{16} backbone. (Note: R denotes C_nH_{2n+1}, Q denotes C_nH_{2n}, Q′ denotes C_nH_{2n-1}.) The γ-ketohydroperoxide, with the C=O and C−OOH functional groups separated by one $-CH_2-$ group, was found to be the most abundant isomer of HOOQ′=O formed in these experiments. Korcek and co-workers also proposed pathways for the formation of these products, starting from the parent

Received: April 7, 2013
Published: July 17, 2013

   dx.doi.org/10.1021/ja4034439 | J. Am. Chem. Soc. 2013, 135, 11100−11114

alkane and proceeding along the R• $\xrightarrow{+O_2}$ ROO• → •QOOH $\xrightarrow{+O_2}$ HOOQOO• → HOOQ′=O + •OH reaction sequence, which is consistent with modern views of low-temperature gas-phase oxidation.[8] They also performed detailed analyses of secondary oxidation products formed by cleavage of the parent hydrocarbon chain, the most important of these products being carboxylic acids and methyl ketones. Commonly assumed pathways for the formation of acids and carbonyl compounds include β-scission of alkoxy radicals (RO•) and the Baeyer−Villiger reaction.[6] However, Korcek and co-workers noted that those pathways alone could not account for the measured organic acid yield.

In order to better understand the origin of carboxylic acids and methyl ketones in the hexadecane oxidation system, Korcek and co-workers studied the thermal decomposition of γ-HOOQ′=O species in the 393−453 K temperature range. In these experiments, HOOQ′=O was accumulated *in situ*, and the reaction mixture then was treated with excess antioxidant (butylated hydroxytoluene, BHT) to suppress free-radical chemistry. The rate of thermal decay of γ-HOOQ′=O was measured by monitoring its concentration after addition of BHT. As γ-HOOQ′=O decomposed, carboxylic acids and methyl ketones were formed. This led Korcek and co-workers to propose a new pathway to acids and methyl ketones via γ-HOOQ′=O, accounting for over half the experimental acid yield. Similar pathways were also used to explain experimental observations in the oxidation of pentaerythrityl tetraheptanoate[7] with effective rate coefficients similar to those measured in the hexadecane system.

Beyond these observations, little is known about the reaction(s) by which γ-HOOQ′=O decomposes to acids and ketones. HOOQ′=O species have only recently been observed experimentally in low-temperature gas-phase oxidation of alkanes,[2,9] and very little is directly known about their properties or reactivity. Interestingly, these experiments also measured high yields of carboxylic acids. Acid formation is unaccounted for in existing combustion models, and this limits their predictive capabilities.

Here we use high-level computational methods to investigate the pathway proposed by Korcek and co-workers. In order to keep the calculations tractable, we examine the case of $HOOCH_2CH_2CHO$, the smallest possible γ-HOOQ′=O. Our investigation reveals that the Korcek reaction involves two elementary steps: the exothermic isomerization of the HOOQ′=O species to a five-membered cyclic peroxide (CP) intermediate followed by concerted fragmentation of this intermediate to give HCOOH + CH_3CHO or CH_3COOH + HCHO. Fragmentation reactions of related cyclic peroxides studied experimentally by Baumstark and Vasquez[10] provide additional evidence for the predicted products. These reactions represent a new general class of reactions and are expected to play an important role in other low-temperature oxidation systems, including biofuel combustion, lipid peroxidation, atmospheric oxidation, and polymer degradation.

2. THEORY AND COMPUTATIONAL METHODS

2.1. Geometries, Frequencies, and Electronic Energies. All stationary points (and their conformers) were optimized using the restricted M06-2X/MG3S electronic model chemistry, where M06-2X is a hybrid meta-GGA density functional[11] and MG3S[12] is a basis set that, for systems containing only H, C, and O, is equivalent to 6-311+G(2df,2p).[13] The M06-2X/MG3S combination has been shown to provide accurate geometries and frequencies for several reaction systems.[14] All M06-2X/MG3S calculations employed a density functional integration grid consisting of 99 radial shells around each atom and 974 angular points in each shell. All calculated vibrational frequencies were scaled by 0.970, a previously determined[15] empirical scale factor for converting harmonic vibrational frequencies obtained with M06-2X/MG3S to best estimates of frequencies to use for calculating zero-point energies. The M06-2X/MG3S geometry optimizations and frequency calculations were carried out using the Gaussian 09 program suite.[16]

Electronic energies of all stationary points and their conformers were refined via single-point calculations with the explicitly correlated RCCSD(T)-F12a[17] method (performed using the Molpro[18] program suite). The F12 family of methods overcomes the slow convergence of conventional CCSD(T) methodologies[19] by introducing explicitly correlated functions into the CC wave function[20] and has been widely applied to both thermochemistry and kinetics[14a,21] calculations with success. Several multireference diagnostics[22] were computed to assess the extent of multireference character of the systems investigated here, and RCCSD(T) was found to provide reliable electronic energies. The corresponding values of these diagnostics are available in Tables S9 and Table S10 along with a detailed discussion. Comparing average barrier heights (from reactions C and F, see Section 3.1) calculated using the cc-pVQZ-F12 basis as benchmark,[23] we found estimates from cc-pVTZ-F12 calculations to lie within 0.25 kcal/mol, while estimates with the cc-pVDZ-F12 basis were found to differ by ∼1 kcal/mol. Based on this, the cc-pVTZ-F12 basis set seemed to provide a good balance between computational cost and accuracy and was used for all subsequent calculations in this work.

Notation. For the remainder of this article, we use the shorthand abbreviation CCSD(T)//M06-2X to denote RCCSD(T)-F12a/cc-pVTZ-F12 energies at M06-2X/MG3S geometries, with scaled M06-2X frequencies. Electronic energy calculations are presented as PES values, that is, they are relative fixed-nuclei energies including nuclear repulsion.

2.2. Partition Functions and Thermal Rate Coefficients. All rate coefficients reported in this article were calculated using multipath variational transition state theory[24] (MP-VTST) with small-curvature tunneling[25] (SCT) (labeled MP-VTST/SCT). MP-VTST/SCT is an improved version of multistructural transition-state theory (MS-TST)[14d,24b,26] that involves a path-averaged transmission coefficient to account for multidimensional tunneling and recrossing effects. MS-TST itself departs from the conventional single-structure (SS) view of TST (labeled SS-TST), where both the reactant(s) and the transition state are represented solely by their lowest-energy conformers with their corresponding partition functions (Q), usually evaluated by the rigid-rotor harmonic oscillator approximation using scaled vibrational frequencies (Q^{SS-QH}) to approximately account for anharmonicity. In cases where flexible molecules adopt multiple stable conformations, which can be quite different from one another, and dynamically interconvert among these, an SS-based formalism does not yield reliable rate coefficients. In MS-TST, single-structural partition functions entering the conventional rate coefficient formula are replaced by partition functions computed by the multi-structural method with torsional anharmonicity[27] (MS-T, $Q^{MS-T}_{con-rovib}$), which sums over partition functions for each structure including corrections for anharmonicity. Applications of $Q^{MS-T}_{con-rovib}$ to derive accurate thermochemistry and kinetics involving flexible molecules have been highlighted in several recent studies.[14d,21b,c,24a,26,28] The MS-T torsional anharmonicity factor for a general species α is defined as follows:

$$F^{MS-T,\alpha} = \frac{Q^{MS-T,\alpha}_{con-rovib}}{Q^{SS-QH,\alpha}_{rovib,1}} \quad (1)$$

where $Q^{SS-QH,\alpha}_{rovib,1}$ is computed at the global minimum. Similarly, the reaction specific torsional anharmonicity factor is defined as:

dx.doi.org/10.1021/ja4034439 | J. Am. Chem. Soc. 2013, 135, 11100−11114

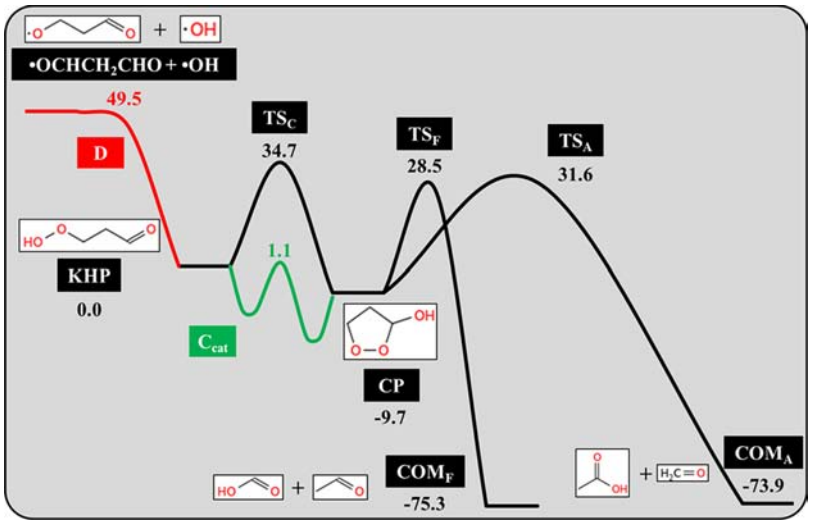

Figure 1. Stationary points on the CCSD(T)//M06-2X potential energy surface for the Korcek reaction sequence starting from $HOOCH_2CH_2CHO$ (KHP). Energies (in kcal/mol) correspond to the lowest-energy conformer of each species relative to the most stable conformer of KHP. Also shown are the homolytic O−O bond dissociation reaction (D) and the acid catalyzed conversion to CP (C_{cat}).

$$F^{\mathrm{MS-T}} = \frac{F^{\mathrm{MS-T},\ddagger}}{\prod_{i=1}^{N_R} F^{\mathrm{MS-T},i}} \tag{2}$$

where i runs over the number of reactants (N_R), and the numerator represents the species-specific F-factor for the transition state (‡).

The optimized geometries, Hessians, scale factor, and refined energies for all conformers were used to generate the necessary input files for the MSTor program[27] to obtain MS-T partition functions, which were subsequently used to calculate thermal rate coefficients using the methods described below. Note that different ring conformations of cyclic structures were taken into account using the multistructural local quasi-harmonic approach.[27b] Details are given in the Supporting Information.

We now move to a brief description of the methodology employed for computing thermal rate coefficients including variational effects, multistructural torsional anharmonicity, and tunneling.[24] For a system with a single saddle point, it is common to compute the rate coefficient using TST using the following equation:

$$k^{\mathrm{SS-TST}} = \kappa\Gamma\frac{k_B T}{h}\frac{Q^{\mathrm{SS-QH},\ddagger}}{\Phi^R}\exp\left(-\frac{V^{\ddagger}}{k_B T}\right) \tag{3}$$

where $Q^{\mathrm{SS-QH},\ddagger}$ is the quantal partition function (including rotational symmetry numbers) of the transition-state structure, Φ^R is the unitless partition function of the reactant for unimolecular reactions or the partition function per unit volume for bimolecular reactions (again including rotational symmetry numbers), and $V^{\ddagger}$ is the classical barrier height. Note that we do not require a reaction-path symmetry number[29] in eq 3 because we have included symmetry numbers in all rotational partition functions. The tunneling correction κ can be computed using multidimensional small curvature tunneling (SCT),[25a,30] and the recrossing factor Γ is conveniently computed using canonical variational transition-state theory.[25b,31]

In our case there are multiple saddle point structures connecting the reactants and products. If the corrections for tunneling and recrossing are small, one can estimate the total rate by

$$k^{\mathrm{MS-TST}} = F^{\mathrm{MS-T}}k^{\mathrm{SS-TST}} \tag{4}$$

For all the reactions considered here, recrossing/tunneling effects were incorporated by computing separate small-curvature tunneling coefficients (κ_k^{SCT}) and recrossing corrections (Γ_k) for each saddle point structure (denoted by subscript k) of a given reaction. The overall MP-VTST/SCT rate coefficient is obtained by combining these calculations as shown below:

$$k^{\mathrm{MP-VTST/SCT}} = F^{\mathrm{MS-T}}k^{\mathrm{SS-TST}}\frac{\sum_{k=1}^{K}\Gamma_k\kappa_k^{\mathrm{SCT}}Q_k^{\mathrm{S},\ddagger}}{\sum_{k=1}^{K}Q_k^{\mathrm{S},\ddagger}} \tag{5}$$

where K is the total number of saddle point structures. In the present work, $k^{\mathrm{SS-TST}}$ values were computed with M06-2X/MG3S geometries and scaled frequencies and CCSD(T)//M06-2X energies using the POLYRATE program.[32] $F^{\mathrm{MS-T}}$ and $Q_k^{\mathrm{S},\ddagger}$ values were computed with M06-2X geometries and scaled frequencies, and CCSD(T)//M06-2X energies using the MSTor computer program.[27a] The calculations of κ_k^{SCT} and Γ_k require Hessians for calculating the minimum energy path and for generalized normal-mode analyses along the path, and this was carried out with the GAUSSRATE program.[33] The MEP was followed in redundant curvilinear (internal) coordinates[34] by using a modified[35] Page−McIver algorithm[36] (where the modification is that a Hessian is computed at only every ninth step, and old Hessians reused at other points) and the reorientation of the dividing surface[37] (RODS) algorithm based on optimizing the orientation of the dividing surface at each point along the reaction path in order to maximize the free energy of the generalized transition state. The advantage of using internal coordinates along the MEP is that it provides more reliable generalized normal-mode frequencies along the MEP than using rectilinear (Cartesian) coordinates.[38] A converged MEP was obtained with a step size of 0.005 Å (with coordinates scaled to a reduced mass of 1 amu). Because of the large computational cost associated with these calculations, the reaction path is calculated with a density functional whose predicted barrier height is close to the best available estimate from high-level calculations (CCSD(T)//M06-2X in this work). This requires additional validation of DFT methods for each reaction as discussed in detail in the Supporting Information. In the following discussion, we lump the multistructural recrossing and tunneling contributions ($\sum_{k=1}^{K}\Gamma_k\kappa_k^{\mathrm{SCT}}Q_k^{\mathrm{S},\ddagger}/\sum_{k=1}^{K}Q_k^{\mathrm{S},\ddagger}$) to $k^{\mathrm{MP-VTST/SCT}}$ and denote the composite factor as $\langle\gamma\rangle^{\mathrm{VTST/SCT}}$.

3. RESULTS

3.1. Potential Energy Surface (PES). The singlet CCSD(T)//M06-2X PES for the Korcek reaction sequence starting from the three-carbon ketohydroperoxide (KHP) is shown in Figure 1. Also shown in Figure 1 are the energetics for the competing homolytic O−O bond dissociation reaction (red, reaction D) and an acid-catalyzed pathway (green, reaction C_{cat}) to cyclic peroxide (CP), both discussed in Section 4. The overall reaction involves two steps: cyclization of KHP into the more stable CP intermediate and fragmentation

dx.doi.org/10.1021/ja4034439 | J. Am. Chem. Soc. 2013, 135, 11100−11114

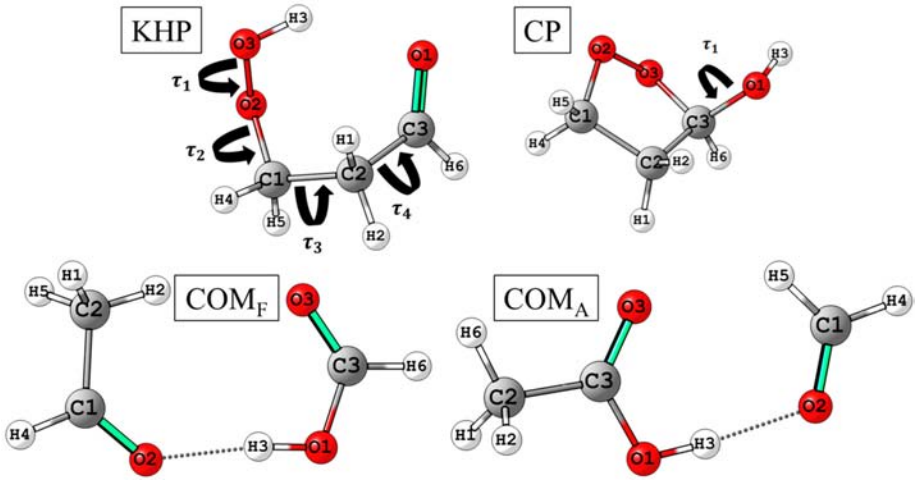

Figure 2. Lowest-energy conformers of all stable species shown on the PES in Figure 1.

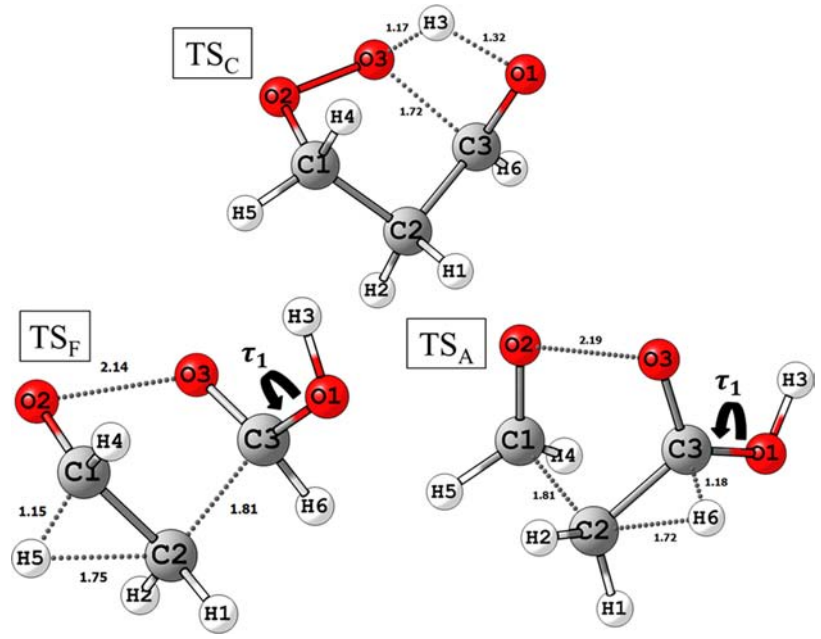

Figure 3. Lowest-energy conformers of transition states shown on the PES in Figure 1. Important bond distances reported in Å.

of CP into acid and carbonyl products. In this section, we qualitatively discuss these chemical transformations using the lowest-energy conformers of all minima and transition states shown in Figures 2 and 3. The corresponding electronic energies (relative to KHP) and zero-point energies are given in Table 1. Details of other possible conformers for each stationary point will be presented in Section 3.2 along with the corresponding MS-T partition functions.

3.1.1. Step 1: Cyclization of KHP. The first step in the Korcek sequence (reaction **C**), involves intramolecular H-atom transfer from the −OOH group (atom H3) in KHP to the carbonyl O-atom (O1), while simultaneously forming a bond between C3 and O3 (TS$_C$ in Figure 3). Snapshots of molecular configurations along the M06-2X/MG3S reaction coordinate (S_C) and the corresponding CCSD(T)//M06-2X energies are shown in Figure 4 (top) and mainly involve formation of the O3−C3 and O1−H3 bonds with simultaneous cleavage of the O3−H3 bond; the corresponding bond distances, *r*, are shown in Figure 4 (bottom). Starting from KHP, the approach to the saddle point (S_C = 0 Å) mainly involves motion of the −OOH group toward the C═O group. At the saddle point, *r*(O3−H3) is stretched by ∼20% from its equilibrium value of 0.96 Å while *r*(H3−O1) = 1.32 Å and *r*(O3−C3) = 1.72 Å (Figure 3). The

Table 1. CCSD(T)//M06-2X Relative Energies, Scaled Zero-Point Energies (both in kcal/mol), and T_1 Diagnostics of Lowest-Energy Conformers for Stationary Points in Figure 1

	species name/reaction	relative energy	ZPE[a]	T_1 diagnostic
KHP	2-formyl ethylhydroperoxide	0.0	59.8	0.014
CP	cyclic peroxide (1,2-dioxolan-3-ol)	−9.7	59.6	0.013
COM$_F$	[formic acid + acetaldehyde]	−75.3	56.2	0.015
COM$_A$	[acetic acid + formaldehyde]	−73.9	56.0	0.015
TS$_C$	KHP ⇌ CP	34.7	56.0	0.017
TS$_F$	CP ⇌ COM$_F$	28.5	54.7	0.017
TS$_A$	CP ⇌ COM$_A$	31.6	54.2	0.018

[a]Zero-point vibrational energy, including scaling.

dx.doi.org/10.1021/ja4034439 | J. Am. Chem. Soc. 2013, 135, 11100−11114

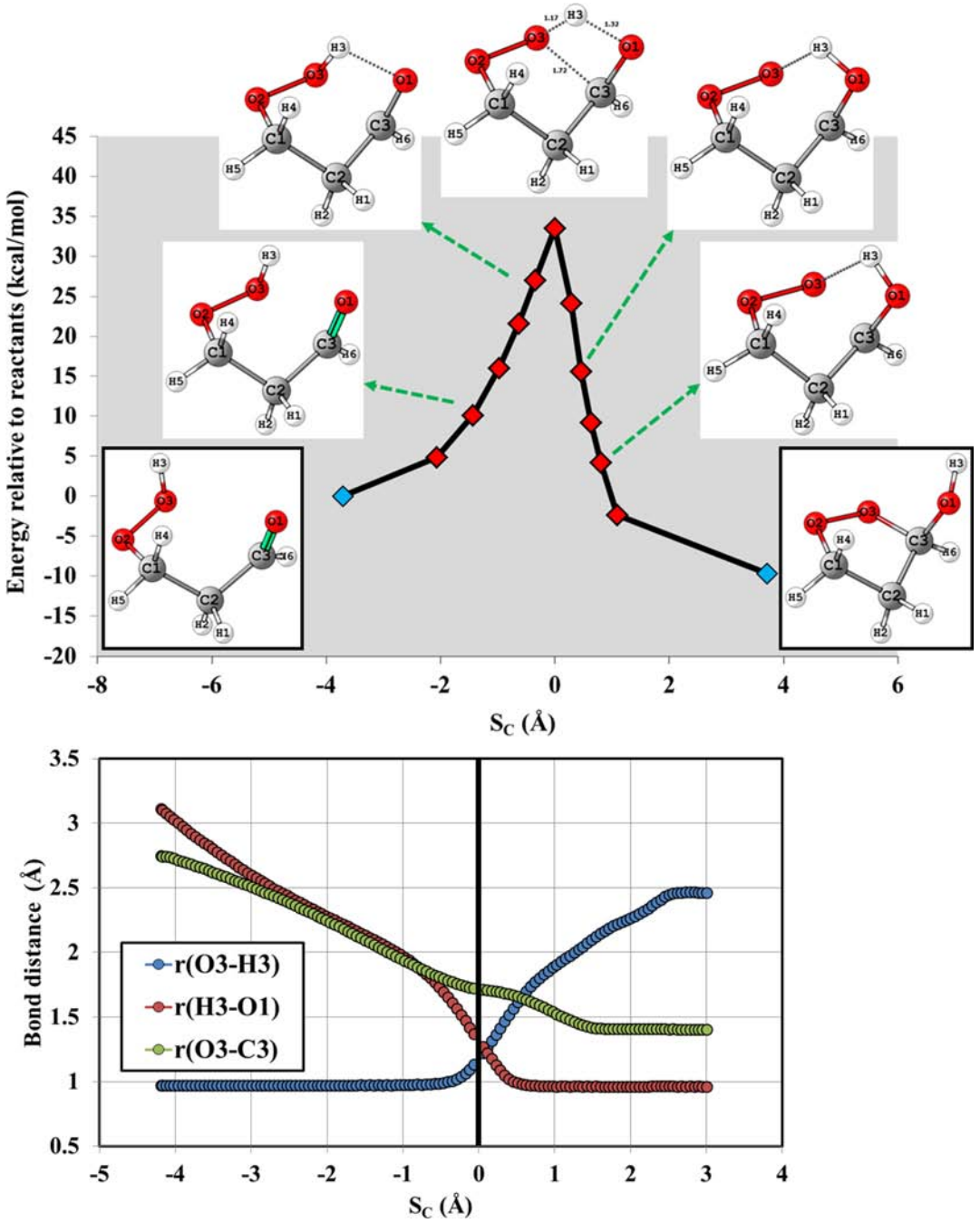

Figure 4. (top) CCSD(T)//M06-2X potential energy along the M06-2X/MG3S minimum energy path (MEP) as a function of the reaction coordinate of reaction **C** (S_C) in isoinertial coordinates scaled to 1 amu. (bottom) Bond lengths (in Å) obtained from geometries along the M06-2X/MG3S MEP.

H-atom transfer from O3 to O1 is accomplished near the saddle point. Meanwhile, r(O3−C3) decreases, and the five-membered ring of CP is formed. The increase in r(O3−H3) after the H-atom is due to internal rotation about the new C3−O1 single bond. The classical barrier ($V^{\ddagger}$) for reaction **C** is 34.7 kcal/mol while the zero-point energy corrected barrier (ΔE_o) is 30.9 kcal/mol. The CP product is energetically more stable than KHP by ∼10 kcal/mol.

3.1.2. Step 2: Fragmentation of the Cyclic Peroxide. The second step in the Korcek sequence is concerted fragmentation of CP into two possible pairs of acid and aldehyde products held together in H-bonded complexes; the two possible reactions are denoted **F** (producing formic acid) and **A** (producing acetic acid). The product and TS structures are shown in Figures 2 and 3. The saddle point TS_A of reaction **A** is shown in Figure 3 and leads to the formation of acetic acid and formaldehyde held together in the second H-bonded complex (COM_A) shown in Figure 2. Both reactions **F** ($V^{\ddagger}$ = 38.2 kcal/mol relative to CP) and **A** ($V^{\ddagger}$ = 41.3 kcal/mol relative to CP) involve very similar changes in bonding. In the following description, we shall confine ourselves to **F**, a similar analysis applies to **A**.

Molecular configurations along the M06-2X/MG3S reaction path for **F** (S_F) and the corresponding CCSD(T)//M06-2X

dx.doi.org/10.1021/ja4034439 | J. Am. Chem. Soc. 2013, 135, 11100−11114

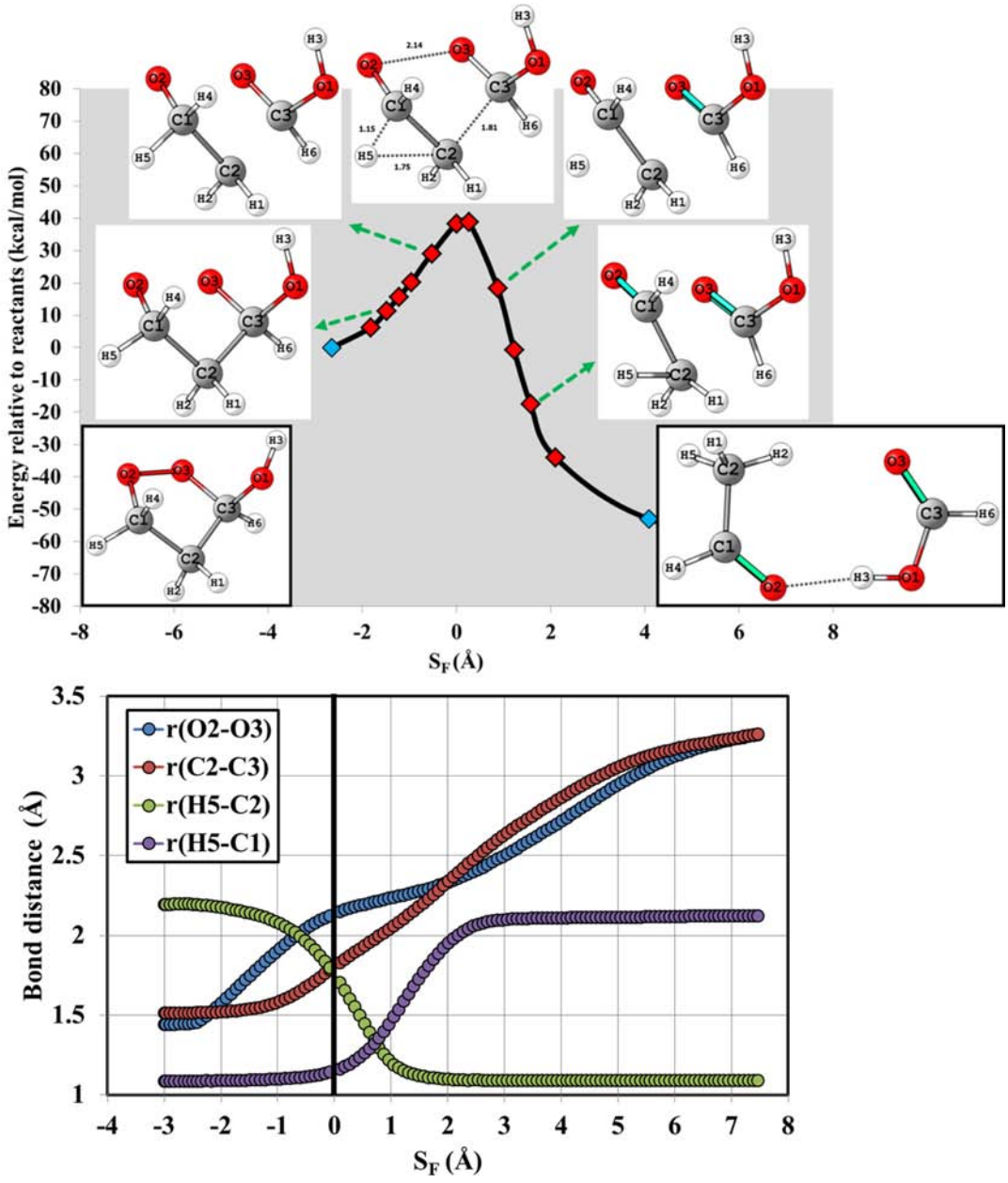

Figure 5. (top) CCSD(T)//M06-2X potential energy along the M06-2X/MG3S minimum energy path (MEP) as a function of the reaction coordinate of reaction **F** ((S_F) in isoinertial coordinates scaled to 1 amu (bottom). Bond lengths (in Å) obtained from geometries along the M06-2X/MG3S MEP.

energies are shown in Figure 5 (top). Fragmentation of CP via **F** involves concerted cleavage of the O2−O3 and C2−C3 bonds accompanied by a 1,2 H-shift of H5 from C1 to C2 leading to HCOOH and CH_3CHO. The main changes in bond lengths along S_F are shown in Figure 5. Starting from CP, the approach to the transition state (S_F = 0 Å) involves a big increase in r(O2−O3), a more modest increase in r(C2−C3) from 1.54 Å to 1.81 Å, and decrease in r(H5−C2) due to decrease in the C2−C1−H5 bond angle. Relatively little change occurs in r(H5−C1) until after the saddle point. Both r(O2−O3) and r(C2−C3) continue to increase beyond the saddle point as double bonds are formed between (C3, O3) and (C1, O2) becoming the carbonyl groups in HCOOH and CH_3CHO. About 80 kcal/mol is released immediately after the saddle point as H5 is transferred and the C═O double bonds form. Later, bond angle and conformational changes as the nascent HCOOH and CH_3CHO adjust further to form the H-bonded complex, COM_F, release about 20 kcal/mol more energy. Including zero-point energy corrections, the overall reaction CP → COM_F has a forward barrier of 33.3 kcal/mol and is 69 kcal/mol exothermic. The variations of r(O2−O3), r(C2−C3), r(H5−C2) and r(H5−C1) along S_F are shown in Figure 5 (bottom).

3.2. Partition Functions and Thermal Rate Coefficients. *3.2.1. Cyclization of KHP via reaction C.* The first step in calculating MS-T partition functions is a comprehensive search for all possible structures. A systematic sampling of the torsional space of KHP yielded 192 initial guesses for torsional conformers, generated from all of the possible combinations between the 4 torsions in this system (marked in Figure 2): 4 torsional values at 90° intervals for torsions τ_1, τ_2, and τ_4, and 3 such values (separated by 120°) for torsion 3 (τ_3). This yielded

dx.doi.org/10.1021/ja4034439 | J. Am. Chem. Soc. 2013, 135, 11100−11114

the expected 54 torsional conformers for KHP (Table S1). The 54 conformations of KHP correspond to 27 pairs of nonsuperimposable mirror image structures.

The five lowest-energy structures (S1−S5 in Table S1) of KHP lie within 1 kcal/mol of each other. The most stable conformer of KHP (S1, Figure 2) is ring-shaped with O1 and H3 separated by 2.15 Å, suggesting stabilization by internal H-bonding. While S1 is lowest in potential energy, inclusion of zero-point energy changes the relative ordering slightly with an acyclic conformation S3 becoming the most stable. Our computed rate coefficients are independent of the choice of reference structure. The M06-2X/MG3S relative energies (Table S1) are in reasonable agreement with the CCSD-(T)//M06-2X energies, although the relative ordering of the conformers is slightly altered. The contribution of torsional and multistructural anharmonicity to KHP partition functions is clearly manifest in the corresponding *F*-factors (Table 2) which lie between 75 and 300 in the temperature range of interest here.

Table 2. Species-Specific Multistructural *F*-factors for All Stationary Points in the Korcek Reaction Sequence As Functions of Temperature

T (K)	KHP	CP	TS_C	TS_F	TS_A	$TS_{C_{cat}}$
300	74.1	4.3	2.0	2.2	2.1	2.6
350	98.6	4.7	2.0	2.3	2.1	2.7
400	124.2	5.0	2.1	2.3	2.2	2.9
450	149.9	5.3	2.1	2.4	2.2	3.0
500	174.9	5.5	2.1	2.6	2.2	3.1
550	198.5	5.8	2.2	2.7	2.2	3.2
600	220.3	6.0	2.2	2.8	2.3	3.3
650	240.3	6.2	2.3	2.9	2.3	3.4
700	258.2	6.4	2.3	3.0	2.3	3.5
750	274.1	6.5	2.4	3.2	2.3	3.6
800	288.0	6.7	2.4	3.3	2.4	3.7

Unlike KHP, the global minimum structure of the ring-shaped transition state for cyclization (TS_C, Figure 3) is fairly rigid with little torsional freedom. However, the seven-membered ring in TS_C can adopt a different conformation (S2 in Table S2), giving rise to another structure (3.3 kcal/mol higher in energy compared to the global minimum) and a total of 4 structures including the nonsuperimposable mirror images.

The MP-VTST/SCT rate coefficients along with reaction specific *F*-factors (F^{MS-T}, eq 2) and generalized transmission coefficients $\langle\gamma\rangle^{VTST/SCT}$ for reaction C are given in Table S11. The corresponding Arrhenius parameters are reported in Table 3. Since $\langle\gamma\rangle^{VTST/SCT}$ calculations are expensive (Section 2.2), we used DFT to approximate the shape of the PES near the saddle point. In choosing the appropriate functional, we took into account that tunneling and recrossing effects depend on the height and width of the barrier in addition to the shape of the Gibbs free energy around the transition state. Details of the DFT validation are available in the Supporting Information. For reaction **C**, combining both criteria we performed the $\langle\gamma\rangle^{VTST/SCT}$calculations using the PBEH1PBE functional in Gaussian 09[16] using a scale factor of 0.975 for the frequencies;[15] this functional is a hybrid version of the PBEhole functional.[39]

Table 3. Arrhenius Parameters (for 300 K < T < 800 K) for Reactions C, F, A, and D in the Gas Phase (High-Pressure Limit)

	reaction	A (s^{-1})	E_a(kcal/mol)
C	KHP ⇌ CP	2.1×10^8	28.0
F	CP ⇌ COM_F	3.4×10^{13}	34.4
A	CP ⇌ COM_A	3.7×10^{13}	36.8
D	KHP ⇌ HO• + •OCH_2CH_2CHO	1.8×10^{16}[a]	43.0[a]

[a]Obtained by refitting rates in the 300−800 K range from modified Arrhenius parameters reported at 100 atm in the gas phase by Goldsmith and co-workers.[62]

3.3. Fragmentation of CP via Reactions F and A. Our conformational search located six low-energy (within 1 kcal/mol) of the global minimum conformers for CP, summarized in Table S3. The conformers arise from two large amplitude motions: pseudorotation of the puckered five-membered ring and internal rotation of the −OH group. It is interesting to note that torsions about the C3−O1 bond in S3 do not give rise to any new conformers at the M06-2X/MG3S level of theory. The resulting *F*-factors for CP are shown in Table 2.

Similar to CP, both TS_F and TS_A have one large amplitude torsional mode (τ_1) about C3−O1 bond (Figure 3) and the potential for different conformations of the puckered five-membered ring. However, CP, TS_F and TS_A each have a different number of stable conformations (Tables S4 and S5). TS_A has a total of 4 structures corresponding to 2 distinct conformers (τ = −7° (S1, Figure 3) and τ_1 = 174° (S2)) connected by torsion and their iso-energetic nonsuperimposable mirror images. TS_F has four distinct conformers. Two structures have ring conformations similar to the CP structure S3 with C1, O2, O3 and C3 in a plane and C2 projecting out of the ring. In addition, TS_F has two other conformers (S3, S4 in Table S4), with O3, C3, C2 and C1 in the same plane and O2 puckering out of the plane. This gives a total of eight structures for TS_F including the iso-energetic nonsuperimposable mirror images of these structures. Computed *F*-factors for both TS_F and TS_A are presented in Table 2. Full details on the MP-VTST/SCT rate calculations for reactions F and A are given in the Supporting Information, see especially Tables S12 and S13. As with reaction **C**, the PBEH1PBE functional was used to build the potential energy surface used for computing the tunneling and variational TST effects. The Arrhenius parameters are given in Table 3. Because the TS_F and TS_A structures are similar to the CP reactant and at the saddle point the reaction coordinate corresponds mostly to heavy atom motion, all the corrections to the SS-TST rate coefficients are modest (factors of two or less). Reaction **F** is computed to be about an order of magnitude faster than reaction **A** due to its lower barrier height.

As noted earlier, current combustion models[2,9] assume that γ-HOOQ′=O species react only via unimolecular O−O bond dissociation (denoted **D** in this work). For comparison, Table 3 also shows gas-phase Arrhenius parameters for **D** using rate coefficients computed recently by Goldsmith and co-workers.[40]

4. DISCUSSION AND IMPLICATIONS FOR KINETIC MODELING

In previous sections, we have provided an overview of the elementary steps involved in the Korcek reaction sequence and computed high-level MP-VTST/SCT rate coefficients in the gas phase. In this section, we add solvent effects to compare with Korcek's measurements (only available experimental rate coefficients for this reaction). In addition, we discuss the

implications of the new pathways for organic acid formation in low-temperature combustion and tropospheric oxidation.

4.1. Solvent Effects and Comparison with Liquid-Phase Measurements. The Arrhenius parameters in Table 3 correspond to the high-pressure limit in the gas phase while the measurements by Korcek and co-workers were performed in liquid hexadecane. For a meaningful comparison, it is important to account for the effect of the surrounding medium on the computed rate coefficients.

Solvent effects on the rate coefficients were computed using the following expression:[41]

$$\frac{1}{k_{solv}} = \frac{1}{k_{gas}\exp\left(-\frac{\Delta G^{*,\ddagger}_{solv} - \sum_i \Delta G^{*,R}_{solv}}{RT}\right)} + \frac{1}{k_{diff}} \quad (6)$$

where k_{diff} is the diffusion limit, and $\Delta\Delta G^{*,\ddagger}_{solv} = \Delta G^{*,\ddagger}_{solv} - \sum_i \Delta G^{*,R}_{solv}$, the difference in the solvation free energy between the transition state and the reactants using the Ben-Naim fixed-concentration standard state (represented by *).[41b,c,42] In the present study, $\Delta\Delta G^{*,\ddagger}_{solv}$ was estimated from single-point calculations using the IEFPCM,[43] CPCM,[44] and SMD[45] continuum solvation models and $k_{gas}(T)$ from the Arrhenius parameters in Table 3. IEFPCM calculations were performed using HF/6-31G+, and CPCM calculations were carried out with HF/6-31G(d), both with UAHF radii, consistent with the recommendations of Ho and co-workers.[46] SMD calculations[45,47] were performed with M06-2X/6-31G(d,p).[45] The PCM calculations include electrostatics, cavitation, dispersion, and repulsion,[44] while SMD calculations include bulk electrostatics and cavitation, dispersion, and solvent structure (CDS) terms.[45,47] Among the reactions of interest here, only **D** is diffusion limited, and the corresponding k_{diff} was estimated using the Smoluchowski formula (see Supporting Information for details). Calculations were performed in three solvents with substantially different dielectric constants: heptane (ϵ = 1.9), chlorobenzene (ϵ = 5.6), and acetonitrile (ϵ = 36.6) to probe the sensitivity of the reaction rate to solvent polarity. $\Delta\Delta G^{*,\ddagger}_{solv}$ values from these calculations for **C**, **F**, and **A** are summarized in Table 4. Reaction **C** depends only weakly on solvent polarity. In contrast, $\Delta\Delta G^{*,\ddagger}_{solv}$ for both CP fragmentation channels (**F** and **A**) show a marked increase with solvent polarity. Both reactions are accelerated in polar media due to the large difference in dipole moments between CP (μ = 2.2 D) and the corresponding transition states ($\mu(TS_F)$ = 4.1 D, $\mu(TS_A)$ = 4.2 D). The numbers in parentheses in Table 4, which represent the electrostatic component of $\Delta\Delta G^{*,\ddagger}_{solv}$, account for a large part of the variation in $\Delta\Delta G^{*,\ddagger}_{solv}$ between solvents for both reactions. Using the CPCM model, $\Delta\Delta G^{*,\ddagger}_{solv}$(**F**) decreases from −1.8 kcal/mol in heptane to −5.5 kcal/mol in acetonitrile with a similar variation in $\Delta\Delta G^{*,\ddagger}_{solv}$(**A**). Both IEFPCM and SMD predict trends and values similar to those obtained by CPCM. For the present calculations, we assume that the solvent in Korcek's experiments behaves like heptane, and we use the average of IEPFCM, CPCM, and SMD values of $\Delta\Delta G^{*,\ddagger}_{solv}$ for computing solvent effects on rate coefficients.

Since reaction **D** occurs via a loose transition state, solvent effects were approximated using the difference in solvation energies between the products and reactants, $\Delta\Delta G^{*,\ddagger}_{solv} \approx \Delta\Delta G^{*,P}_{solv} = \sum_i \Delta G^{*,P}_{solv} - \sum_i \Delta G^{*,R}_{solv}$ in eq 6 using heptane as the model solvent. The mean value of $\Delta\Delta G^{*,P}_{solv}$ using the IEFPCM, CPCM, and SMD models and M06-2X/MG3S optimized geometries of the dissociation products (shown in Supporting

Table 4. $\Delta\Delta G^{*,\ddagger}_{solv}$ (in kcal/mol) at 298 K for Reactions C, F and A, Computed Using IEFPCM, CPCM, and SMD Solvation Models[a]

	IEFPCM[b]			CPCM[c]			SMD[d]		
solvent	C	F	A	C	F	A	C	F	A
heptane (ϵ = 1.9)	−0.7 (−0.2)	−1.3 (−1.8)	−1.3 (−1.9)	−0.8 (−0.2)	−1.8 (−2.3)	−1.8 (−2.5)	−0.2 (0.0)	−1.9 (−1.6)	−1.9 (−1.6)
chlorobenzene (ϵ = 5.6)	−1.0 (−0.3)	−3.5 (−4.1)	−3.5 (−4.2)	−1.0 (−0.3)	−3.9 (−4.5)	−4.0 (−4.7)	−0.1 (0.1)	−3.6 (−3.5)	−3.6 (−3.4)
acetonitrile (ϵ = 36.6)	−1.2 (−0.4)	−4.8 (−5.4)	−5.0 (−5.7)	−1.2 (−0.4)	−5.5 (−4.9)	−5.1 (−5.8)	0.0 (0.2)	−4.2 (−5.0)	−4.2 (−4.9)

[a]Numbers in parentheses correspond to the electrostatic component of $\Delta\Delta G^{*,\ddagger}_{solv}$. [b]IEFPCM/HF/6-31+G*//M06-2X/MG3S calculations with the UAHF radii. [c]CPCM/HF/6-31+G(d)//M06-2X/MG3S calculations with the UAHF radii. [d]SMD/M06-2X/6-31G(d,p)//M06-2X/MG3S calculations.

dx.doi.org/10.1021/ja4034439 | J. Am. Chem. Soc. 2013, 135, 11100−11114

Information) was found to be −0.7 kcal/mol. The acceleration in **D** due to polarity related solvent effects is compensated by diffusion-controlled limitation of the reverse bimolecular association reaction. In the 393−453 K range, diffusive limitations lower $k(\mathbf{D})$ by a factor varying between 3 and 5 (see Supporting Information).

Before comparing estimated rate coefficients with Korcek's measurements, it is important to recognize the role of the KHP ↔ CP equilibrium in determining the relative contribution of **D**, **F**, and **A** to the overall kinetics of KHP consumption. As mentioned earlier, the electronic energy of CP is 9.7 kcal/mol lower than KHP in the gas-phase and the energy gap further increases to 10.3 kcal/mol in alkane solvent. At the low temperatures in Korcek's experiments, CP formation is expected to be thermodynamically favored. However, the time required to establish the equilibrium distribution will depend on the kinetics of cyclization. In the case of slow cyclization, very little CP will be formed to react via **F** or **A**, and KHP decomposition will be dominated by **D**. In the case of rapid interconversion between KHP and CP, which is expected in Korcek's experiments (discussed later), the contribution of **D** to the total rate of consumption will be proportional to the fractional population of KHP, while that of **F** and **A** will be proportional to the fractional population of CP. At a given temperature T, these fractional populations can be expressed in terms of the equilibrium constant ($K_{eq} = [CP]_{eq}/[KHP]_{eq}$) as $f(KHP) = 1/(K_{eq} + 1)$ and $f(CP) = K_{eq}/(K_{eq} + 1)$. The rate coefficients of **D**, **F**, and **A** should be multiplied by these fractional populations to make meaningful comparisons with Korcek's data.

In Table 5, we report solvent-corrected rate coefficients for **C**, **D**, and (**F** + **A**) in the nonequilibrium case along with the

Table 5. Experimental KHP Decomposition Rates (s^{-1}) Reported by Korcek and Co-Workers and Theoretical Estimates of Rate Coefficients for D, C, and F + A[a]

	theoretical estimates			
T (K)	cyclization (C)	dissociation (D)	fragmentation (F + A)	experiment
393	1.2×10^{-7}	9.6×10^{-9}	2.4×10^{-5}	4.5×10^{-5}
433	3.1×10^{-6}	2.1×10^{-6}	1.2×10^{-3}	1.6×10^{-3}
453	1.3×10^{-5}	2.1×10^{-5}	6.4×10^{-3}	7.1×10^{-3}

[a]Solvent contributions are included for reactions C, F, and A by using mean $\Delta\Delta G^{*,\ddagger}_{solv}$ values from Table 4 in eq 6. Solvent contributions for reaction D include polarity and diffusion limitations; see text.

experimental γ-HOOQ′=O decomposition rates reported by Korcek and co-workers at 393, 433, and 453 K. We see that $k(\mathbf{D})$ is 300−5000 times slower than the experimental decay rate at the temperatures of interest. Our calculations indicate cyclization is the rate-limiting step in the KHP ↔ CP →[acid + carbonyl] reaction sequence. The rate coefficient $k(\mathbf{C})$ itself is too low to explain the experimental decay as $k(\text{expt.})/k(\mathbf{C})$ varies between 375 (at T = 393 K) and 550 (at T = 453 K). These discrepancies are significant, probably too large to be due to approximations in the computations. This rules out the nonequilibrium case as a plausible explanation of Korcek's experiments.

Korcek and co-workers proposed that the formation of CP should be rapid and that the experimentally observed decay corresponds to the rate-limiting fragmentation of CP. In Table 6, we report theoretical values for K_{eq} and predicted rates if

Table 6. Experimental KHP Decomposition Rates (s^{-1}) Reported by Korcek and Co-Workers and Theoretical Estimates for D and F + A Rate Coefficients Weighted by Equilibrium Fractional Populations of KHP and CP[a]

	theoretical estimates			
T (K)	equilibrium constant ($K_{eq} = [CP]_{eq}/[KHP]_{eq}$)	dissociation ($k(\mathbf{D})/(K_{eq} + 1)$)	fragmentation ($k(\mathbf{F} + \mathbf{A})K_{eq}/(K_{eq} + 1)$)	experiment
393	425.5	2.3×10^{-11}	2.4×10^{-5}	4.5×10^{-5}
433	122.7	1.7×10^{-8}	1.2×10^{-3}	1.6×10^{-3}
453	71.5	2.9×10^{-7}	6.3×10^{-3}	7.1×10^{-3}

[a]Solvent contributions are included for reactions C, F, and A by using mean $\Delta\Delta G^{*,\ddagger}_{solv}$ values from Table 4 in eq 6. Solvent contributions for reaction D include polarity and diffusion limits.

KHP ↔ CP equilibrium is fast, i.e., rates for **D** and (**F** + **A**) weighted by the fractional populations of KHP and CP, respectively. Since CP is highly favored thermodynamically (as was predicted by Korcek and co-workers), the overall contribution of reaction **D** to KHP decomposition is rather small at the temperatures in Korcek's experiments. The experimental decay and the computed total weighted fragmentation rates (**F** + **A**) are in excellent agreement, with the ratio between them varying between 1.1 and 1.8 in the 393−453 K temperature range (Table S15).

In the low-temperature conditions in Korcek's experiments even small errors in barrier heights can have large effects on rate coefficients. RCCSDT and RCCSDT(2)$_Q$ calculations show that our barrier height is converged with respect to electron correlation to within about 1 kcal/mol (Table S10). There is also some uncertainty in our computed A factor and solvent effects. We estimate a total uncertainty of about a factor of 10 in the estimated rate coefficients at these low temperatures. There must also be significant uncertainties in the experimental data, so we think it is fortuitous that our calculations agree so precisely with the experiment.

The data in Tables 6 and 7 provide strong evidence for rapid equilibrium between KHP and CP followed by decomposition

Table 7. Variation of Critical Carboxylic Acid Concentrations (at Which k(F+A) and $k(C_{cat})$ Are Equal) with Temperature[a]

T (K)	fragmentation ($k(\mathbf{F} + \mathbf{A})K_{eq}/(K_{eq} + 1)$)	acid catalyzed cyclization, $k(C_{cat})$ ($cm^3\ mol^{-1}s^{-1}$)	$[acid]_{critical}$[b] (mol/cm^3)
393	2.4×10^{-5}	3.3×10^{6}	7.3×10^{-12}
433	1.2×10^{-3}	2.8×10^{6}	4.3×10^{-10}
453	6.3×10^{-3}	2.7×10^{6}	2.3×10^{-9}

[a]Above these concentrations, KHP decomposition via HOOQ=O ↔ CP → acid + carbonyl sequence is rate-limited by CP fragmentation reactions (F + A). [b]Defined as $k(F + A)K_{eq}/k(C_{cat})(K_{eq} + 1)$.

via **F** and **A** in Korcek's experiments. While our calculations confirm that the CP is energetically stable compared to KHP (Table 1), the unimolecular route to CP is too slow for **F** and **A** to be rate-limiting. A possible explanation for this discrepancy is the presence of lower-energy pathways for the KHP ↔ CP isomerization process. Recently, da Silva[48] showed that carboxylic acids, like HCOOH, can catalyze keto−enol tautomerization. The reaction involves barrierless formation of a prereaction complex between the acid and the aldehyde followed by a double-hydrogen shift (DHS) reaction between the C and O terminals of the aldehyde and the two O atoms of

dx.doi.org/10.1021/ja4034439 | J. Am. Chem. Soc. 2013, 135, 11100−11114

the carboxylic acid. The reaction leads to no net change in carboxylic acid concentration and converts the aldehyde into the corresponding enol. The barrier height of the catalyzed process was found to be significantly lower than the unimolecular tautomerization process which involves 1,3 H-shift via a four-membered ring-shaped transition state. Other oxygenated species, like water, were also found to act as catalysts, but their activity was significantly lower than carboxylic acids.[48]

Like keto−enol tautomerization, the unimolecular cyclization of KHP (reaction **C**) involves a high-barrier internal H-atom transfer and is likely to be catalyzed by carboxylic acids. For our investigations, we chose the smallest organic acid (HCOOH), but it is reasonable to expect similar results with other acids. Figure 6 shows the lowest-energy structure of the transition

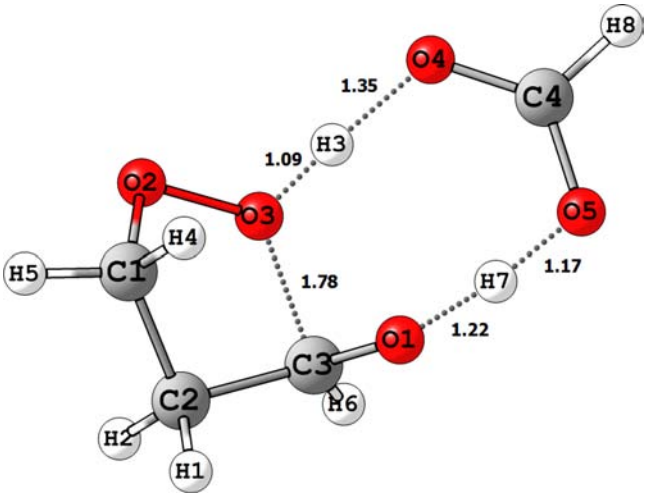

Figure 6. M06-2X/MG3S optimized transition state for the formic acid (HCOOH) catalyzed KHP ↔ CP isomerization ($TS_{C_{cat}}$). Important bond distances (in Å) are shown.

state for the HCOOH catalyzed KHP ↔ CP isomerization (denoted $\mathbf{C_{cat}}$) optimized using the M06-2X/MG3S model chemistry. The corresponding PES is similar to the one reported by da Silva for keto−enol tautomerization and involves formation of a prereaction complex between KHP and HCOOH. This is followed by a double-hydrogen exchange reaction in which HCOOH donates the acidic H (H7 in Figure 6) to the carbonyl O-atom (O1) on KHP. Simultaneously, HCOOH accepts H3 from the −OOH group on KHP at the carbonyl O-atom (O3), while the C3−O3 bond distance decreases. The product is a CP-HCOOH H-bonded complex, lower in energy than the KHP-HCOOH complex owing to the higher stability of CP compared to KHP. The barrier height for $\mathbf{C_{cat}}$ starting from the lowest-energy conformers of KHP and HCOOH was found to be only 0.5 kcal/mol at the CCSD(T)//M06-2X level of theory, which is much lower than the corresponding value (34.7 kcal/mol) for the unimolecular cyclization route (**C**).

Rate coefficient calculations for C_{cat} in the 300−800 K temperature range were performed using the methods described in Section 2.2 and are summarized in Table S14. As seen in Figure 6, $TS_{C_{cat}}$ is fairly rigid and has no torsional degrees of freedom. However, like TS_C, it has one additional structure (S2, Table S6) due to a different conformation of the ring which gives a total of four structures including the isoenergetic nonsuperimposable mirror images. *F*-factors for HCOOH were computed including the syn (global minimum) and anti conformers (Table S7) connected by torsion about the C−O bond (see Table S14 for *F*-factors of $TS_{C_{cat}}$ and HCOOH). The *F*-factors for the overall reaction (F^{MS-T} (*T*), Table S14) were computed using *F*-factors for KHP (Table 2), HCOOH and $TS_{C_{cat}}$. It is worth noting that $F^{MS-T}(T)$ values are very similar to corresponding values for reaction **C** as both involve accessing rigid transition structures starting from a more flexible KHP molecule. CCSD(T)//M06-2X energies for the lowest-energy conformers of KHP, HCOOH, and $TS_{C_{cat}}$ were used to calculate $V^{\ddagger}$ for use in eq 3. The resulting *k*(MP-VTST/SCT) rate coefficients are shown in Table S14. The simple Arrhenius form was found to accurately fit the calculated rate coefficients with $A = 6.3 \times 10^5$ cm^3 mol^{-1} s^{-1} and $E_a = -1.3$ kcal/mol.

While C_{cat} provides a low-energy bimolecular route for the KHP ↔ CP isomerization, the total flux through this pathway depends on the concentration of acid in the surrounding medium. In Table 7, we compute the acid concentrations at which the bimolecular cyclization rate ($\mathbf{C_{cat}}$) and the total fragmentation rate coefficients (**F** + **A**) are equal. These values represent the *critical concentration* of acid for fragmentation to be rate limiting at the temperatures of interest. As seen in Table 7, even μM quantities of acid are sufficient for the cyclization rate to overtake fragmentation with smaller concentrations required at lower temperatures. At 453 K, the critical acid concentration is about 250 times smaller than the lowest experimental acid yield measured by Korcek and co-workers (corresponding to 590 μM at 0.3% conversion of hexadecane). Even if alternative pathways (e.g., Baeyer−Villiger oxidation) contributed only 1% of the total acid yield, they would still produce enough acid for KHP to isomerize rapidly into its more stable CP isomer activating the Korcek reaction sequence. Moreover, any acids produced via the Korcek pathway can themselves act as catalysts, hence making the overall pathway *autocatalytic*. In addition to carboxylic acids, assisted isomerization reactions should also be possible with other oxidation products, like H_2O, aldehydes, ROOH (including the KHP self-reaction, whereby the −OOH functional group on one KHP molecule and the carbonyl functional group in another KHP molecule participate in a double hydrogen shift reaction leading to the formation of two CP molecules, i.e., 2 KHP → 2CP) with varying catalytic activities as also reported by da Silva for keto−enol tautomerization.

Consequently, in the liquid-phase experiments of Korcek and co-workers, it is likely that the γ-HOOQ′=O species interacted with the surrounding oxidation products rapidly isomerizing into CP which underwent subsequent fragmentation reactions. Catalyzed KHP↔CP isomerization might also explain the inhibition of oxidation (due to suppression of radical-forming reaction **D**) observed when carried out in the presence of small quantities of acids.

Even though our theoretical estimates for the concerted fragmentation reactions combined with solvent effects are in excellent agreement with Korcek's measurements, competing alternate reaction paths, e.g., a two-step mechanism going through the biradical intermediate, cannot be ruled out. Little is known theoretically about ring-opening reactions of cyclic peroxides with five or more atoms in the ring. As a result, the fragmentation rate coefficients reported here represent lower bounds on the overall decomposition rate of CP. This reaction

dx.doi.org/10.1021/ja4034439 | J. Am. Chem. Soc. 2013, 135, 11100−11114

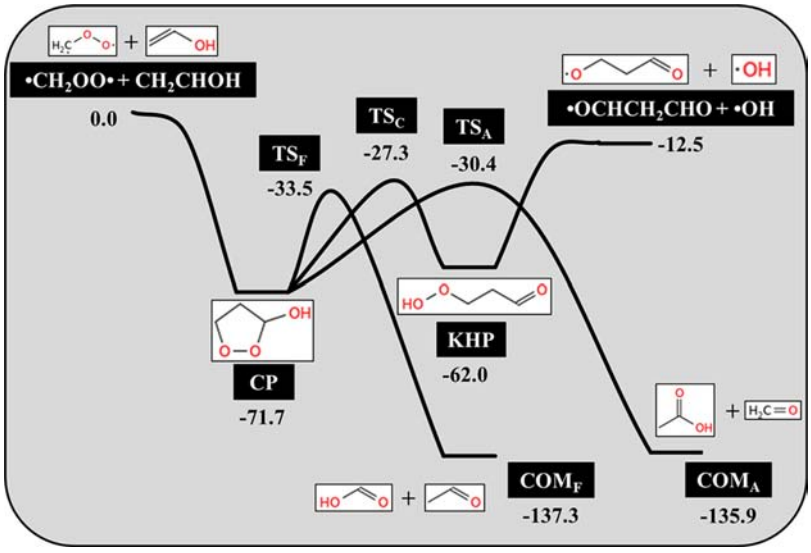

Figure 7. CCSD(T)//M06-2X potential energy surface for •CH_2OO• + CH_2=CHOH. Potential energies (in kcal/mol) correspond to the lowest-energy conformer of each species relative to infinitely separated reactants.

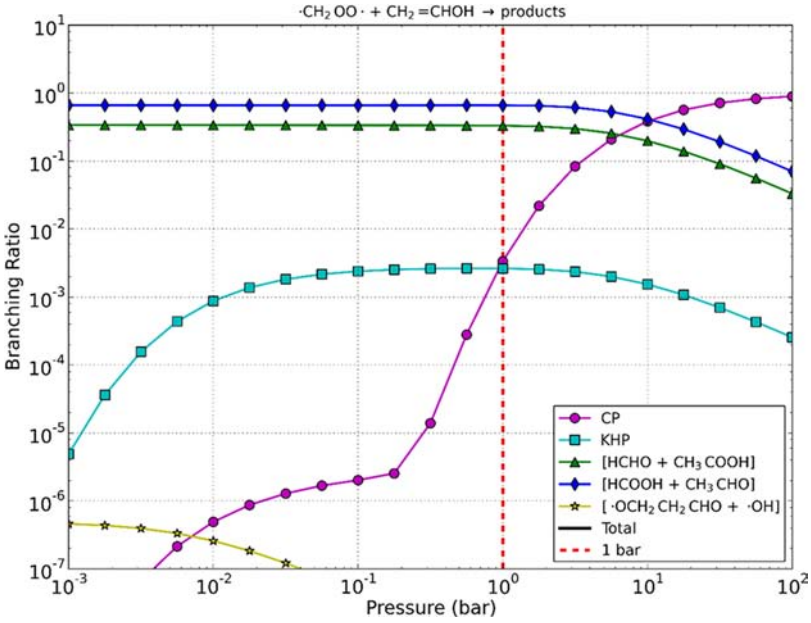

Figure 8. Master equation predictions for the product branching in the reaction between •CH_2OO• and CH_2=CHOH as a function of pressure at 298 K.

path explains the high yields of methyl ketones observed by Korcek and co-workers, and the presence of alternative routes to carboxylic acids is perhaps the most significant implication of the Korcek reaction for liquid-phase oxidation models since these have been attributed exclusively to Baeyer–Villiger oxidation of aldehydes for decades.[6,49]

4.2. Enols as a Potential Source of Acids in the Atmosphere. Kinetic models of secondary organic aerosol formation often under-predict yields of carboxylic acids.[50] Archibald and co-workers[51] recently proposed enols as a potential source of acids citing reactions with the •OH radical followed by reactions with NO, NO_3, HO_2, and O_2 yielding formic acid among other products. The work of Andrews and co-workers[50] on phototautomerization of aldehydes provides further evidence for the formation of enols in the troposphere and their subsequent transformation to organic acids. Enols have also been shown to be important intermediates in combustion chemistry by Taatjes and co-workers,[52] who also recently carried out studies on reactions of the Criegee biradical (•CH_2OO•) with aldehydes and ketones to demonstrate that these could be a potential source of acids at low temperatures and pressures.[53] Reactions between enols and •OH have been studied theoretically[54] (exhibiting significant difficulties due to MR character), but reactions of enols with •CH_2OO• have never been investigated; here we provide theoretical evidence for this channel as a potential source of acids under atmospheric conditions using vinyl alcohol (CH_2=CHOH) as a representative enol.

The connection between •CH_2OO•, CH_2=CHOH, and the Korcek reaction sequence comes from the fact that the CP intermediate can also be formed from 1,3-cycloaddition of •CH_2OO• across the C=C bond in CH_2=CHOH. Starting

dx.doi.org/10.1021/ja4034439 | J. Am. Chem. Soc. 2013, 135, 11100–11114

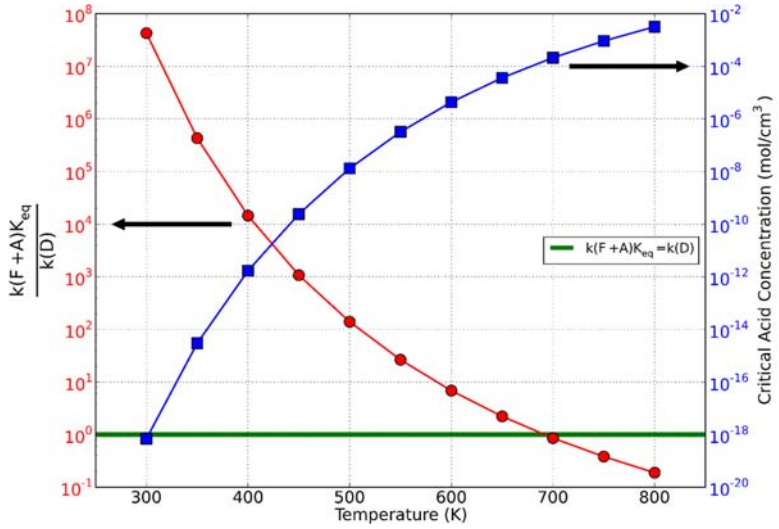

Figure 9. Ratio of fragmentation to dissociation ($k(\mathbf{F} + \mathbf{A})K_{eq}/k(\mathbf{D})$) assuming KHP↔CP equilibrium, and critical carboxylic acid concentration ($k(\mathbf{F} + \mathbf{A})K_{eq}/k(\mathbf{C_{cat}})(K_{eq} + 1)$) in the gas phase as a function of temperature.

from •CH_2OO• and CH_2=CHOH at infinite separation, the CP intermediate is about 72 kcal/mol lower in energy as seen in the PES in Figure 7, while the decomposition channels **F** and **A** lie more than 30 kcal/mol below the entrance channel. At low pressures, reaction between •CH_2OO• and CH_2=CHOH can result in chemically activated decomposition of the CP intermediate resulting in the formation of acids.

For this study, RRKM master equation calculations were performed using the latest version of the CanTherm software package.[55] CCSD(T)//M06-2X energies and scaled M06-2X/MG3S frequencies for all points on the •CH_2OO• + CH_2=CHOH PES (Figure 7, see Supporting Information for M06-2X/MG3S optimized geometries of •CH_2OO• and CH_2=CHOH) were used along with the reservoir state method of Green and Bhatti[56] to obtain $k(T,P)$ values. In addition to decomposition via **F** and **A**, Figure 7 also includes isomerization to KHP (reverse of reaction **C**) and its subsequent decomposition via reaction **D**. Torsional anharmonicity effects were considered only for KHP (which has four torsions) using the separable-rotor approximation (Table S8), as densities of states corresponding to MS-T partition functions have not yet been implemented into master equation software. Torsional anharmonicity and tunneling effects were ignored for other species and reactions since their contribution to the high-pressure limit rate coefficients was small. The bimolecular rate coefficient for the loose entrance channel (•CH_2OO• + CH_2=CHOH ↔ CP) was set at 1×10^{12} $cm^3/mol{\cdot}sec$.[48] A single-exponential down model was used to represent the collisional energy-transfer probability with the energy-transfer parameter modeled as $\Delta E_{down} = 150(T/300)^{0.85} cm^{-1}$ to account for its weak temperature dependence. The collision frequency was estimated using a Lennard-Jones (LJ) model, with LJ parameters of σ = 5.52 Å and ε = 325.09 K for CP and σ = 5.89 Å and ε = 280.14 K for KHP based on group additivity estimates.[57] The nitrogen bath gas LJ-parameters, σ = 3.68 Å and ε = 97.7 K, were taken from literature.[58]

Pressure-dependent branching fractions at 298 K for the total •CH_2OO• + CH_2=CHOH reaction, collisional stabilization into CP, isomerization to KHP and chemically activated formation of [HCOOH + CH_3CHO], [HCHO + CH_3COOH], and •OCH_2CH_2CHO + •OH, are shown in Figure 8. The master equation predictions suggest that acids are the major products at pressures below 10 bar. The lower barrier of channel **F** results in higher yield of [HCOOH + CH_3CHO] (more stable isomers of •CH_2OO• and CH_2=CHOH respectively) compared to that of [HCHO + CH_3COOH] formed via channel **A**. At 298 K and 1 bar (dashed red line in Figure 8), the rate coefficient for total acid production was predicted to be about 300 times higher than the next highest rate coefficients corresponding to collisional stabilization into CP or isomerization into KHP. The yield of •OCH_2CH_2CHO + •OH was found to be negligible at all pressures considered here. This confirms the •CH_2OO• + CH_2=CHOH reaction as a viable source of organic acids in the troposphere. Pressure-dependent rate coefficients (in Chebyshev format)[59] for the •CH_2OO• + CH_2=CHOH reaction for use in atmospheric chemistry models are available in the Supporting Information.

Similar pathways may be also be responsible for the acid products seen in the recent low-pressure experiments on reactions between •CH_2OO• and acetaldehyde performed by Taatjes and co-workers.[53a] These experiments provide evidence for the formation of acetic acid, most likely formed by chemically activated decomposition of the secondary ozonide intermediate formed by addition of •CH_2OO• across the carbonyl double bond and bearing a strong structural resemblance to the CP intermediate in the Korcek reaction. In addition, KHPs themselves are thought to be important intermediates in secondary organic aerosol formation,[60] but our results suggest that they are likely to convert to cyclic peroxides in aerosols containing carboxylic acid groups. To our knowledge, the environmental fate of cyclic peroxides is so far unknown.

4.3. Formation of Acids in Low-Temperature Combustion. Recently, Battin-Leclerc and co-workers performed a series of low-temperature gas-phase oxidation studies on propane,[9a] butane[9b] and *n*-heptane[2] in a jet-stirred reactor and provided conclusive evidence for the formation of carboxylic acids in these systems. Most low-temperature combustion models do not predict acid formation and assume **D** to be the main channel for KHP consumption. Even though the activation energy for reaction **C** is significantly lower than that for **D**, its low *A* factor has a compensating effect. Gas-phase

dx.doi.org/10.1021/ja4034439 | J. Am. Chem. Soc. 2013, 135, 11100−11114

rate coefficients for reactions **C** and **D** are equal at $T \sim 410$ K, above which we expect **D** to be the dominant unimolecular consumption channel for KHP in the gas phase. The above arguments are reasonable in a scenario where KHP and CP isomerization is not catalytically accelerated but not in the presence of acids. In the presence of even trace amounts of carboxylic acids, as in Korcek's experiments, KHP and CP will be equilibrated and the relative contributions of **D** and (**F** + **A**) will depend on the fractional equilibrium populations of KHP and CP. The values of K_{eq}, weighted contributions of **D** and (**F** + **A**) and critical acid concentration in the gas phase in the 300−800 K temperature range are shown in Table S16. The corresponding ratio of these contributions (K_{eq} k(**F** + **A**)/k(**D**)) is shown in Figure 9. As seen both in Table S16 and Figure 9, in the case of fast KHP ↔ CP equilibrium, the contributions from **D** and (**F** + **A**) are equal around 700 K above which **D** dominates. The autocatalytic nature of the Korcek reaction can result in an induction period during which acid concentration builds slowly until it reaches the critical concentration.

For experiments run at 410 < T < 700 K the relative importance of the Korcek sequence and direct decomposition can be sensitive to experimental details. Steady-state experiments with back-mixing of products, such as in the jet-stirred reactor experiments of Battin-Leclerc and co-workers, will facilitate autocatalytic buildup of acids. At low temperatures (<600 K) trace acid contaminants or wall reactions may be enough to kick off the Korcek sequence. But >650 K, quite high acid concentrations would be required, so for most gas-phase experiments >650 K, we anticipate most of the KHP will follow path D rather than the Korcek sequence. The Korcek reaction may be more important in the oxidation/ignition of some oxygenated fuels like ketones and alcohols,[61] where KHPs can be formed very early in the process.

In addition to the low-temperature oxidation systems described above, the elementary reactions of the Korcek sequence themselves present interesting implications for synthetic and biological oxidation chemistry. The decomposition of CP discussed in this article qualitatively explains the products seen by Baumstark and co-workers[10] in experiments on thermal decomposition of penta-substituted 3-hydroxy-1,2-dioxolanes. Lipid molecules containing C═O moieties are likely to undergo peroxidation in the vicinity of this group in early stages of oxidation.[3,62] At the low temperatures prevalent in biological oxidation,[63] lipids with hydroperoxides γ to the carbonyl group are much more likely to form cyclic peroxides (e.g., via acid catalysis) than decompose to form radicals.

5. CONCLUSIONS

In this work, we employ state-of-the-art electronic structure and computational kinetics methods to provide evidence and theoretical rate coefficients for new pathways in low-temperature oxidation of hydrocarbons, as first hypothesized by Korcek and co-workers over 30 years ago. The new pathways lead to the conversion of KHPs into carboxylic acids and carbonyl compounds that are well-known products in liquid-phase oxidation and have also recently been observed in low-temperature combustion and atmospheric oxidation. The Korcek reaction sequence involves the isomerization of the KHP species to the more stable five-membered cyclic peroxide and can occur via unimolecular and acid-catalyzed bimolecular pathways. The second step in the sequence involves concerted fragmentation of the O−O and C−C bonds in CP accompanied by 1,2 H-shift to directly yield carboxylic acids and carbonyl products. Multiple multireference diagnostics were employed to confirm the likely validity of single-reference CCSD(T)//M06-2X methods for the new set of reactions, and quantum mechanical calculations were used to obtain rate coefficient estimates including solvent effects and tunneling contributions.

Based on our calculations, unimolecular cyclization via reaction **C** was found to be the rate-limiting step in the overall sequence. For gas-phase systems, in the absence of catalyzed cyclization, bond dissociation (**D**) is expected to be the main unimolecular route for KHP consumption at temperatures above 400 K. As oxidation products build up, acid-catalyzed and other lower-energy bimolecular channels are expected to dominate and lead to rapid equilibrium between KHP and CP. Even trace amounts of acids in the reacting mixture can rapidly catalyze the cyclization process making fragmentation of CP the rate-limiting process and leading to the autocatalytic formation of even more acid and carbonyl products. Incorporation of acid-catalyzed cyclization and solvent effects leads to excellent agreement between theoretical predictions and the limited experimental data reported by Korcek and co-workers.

In addition to liquid-phase oxidation (corresponding to the high-pressure limit with solvent effects), the new pathways are also relevant in gas-phase ozonolysis chemistry which operates at substantially lower pressures. Preliminary master equation calculations suggest that the chemically activated decomposition of CP formed by reaction between the Criegee intermediate and vinyl alcohol can lead to formation of organic acids (underestimated by existing kinetic models) under atmospheric conditions. The new pathways qualitatively explain acid formation in recent low-temperature alkane combustion experiments in jet-stirred reactors and are also expected to be relevant in lipid peroxidation chemistry.

■ ASSOCIATED CONTENT

Supporting Information

Relative energies (in kcal/mol) and absolute energies (in hartrees) calculated by M06-2X/MG3S and CCSD(T)//M06-2X, scaled zero-point energies and Cartesian coordinates of all stationary points and their conformers, diffusive limits on reaction **D**, F-factors for KHP from separable rotor approximation, overall temperature-dependent KHP decomposition rates in the gas phase with comprehensive technical details, comparison of MEP curves for reactions **C** and **F** calculated by DFT and CCSD(T)//M06-2X, detailed discussion of multireference diagnostics, validation of DFT functionals for $\langle\gamma\rangle^{VTST/SCT}$ calculations, thermal rate coefficients corresponding to individual saddle point structures and CHEMKIN-compatible pressure-dependent rate coefficients for the •CH_2OO• + CH_2═CHOH reaction. This material is available free of charge via the Internet at http://pubs.acs.org.

■ AUTHOR INFORMATION

Corresponding Author

whgreen@mit.edu; truhlar@umn.edu

Present Address

[§]Hydrotex, 12920 Senlac Dr. STE 190, Farmers Branch, Texas 75234, United States.

Notes

The authors declare no competing financial interest.

■ ACKNOWLEDGMENTS

The authors thank Dr. Jingjing Zheng and J. W. Allen for helpful discussions. This work is supported by the U.S. Department of Energy, Office of Basic Energy Sciences under the Energy Frontier Research Center for Combustion Science (grant no. DE-SC0001198). This work was also supported in part by computing time grants from the Molecular Science Computing Facility at the Environmental Molecular Sciences Laboratory of Pacific Northwest National Laboratory and from Minnesota Supercomputing Institute.

■ REFERENCES

(1) Denisov, E. T.; Afanas'ev, I. B. *Oxidation and Antioxidants in Organic Chemistry and Biology*; CRC Press: Boca Raton, FL, 2005.
(2) Herbinet, O.; Husson, B.; Serinyel, Z.; Cord, M.; Warth, V.; Fournet, R.; Glaude, P.-A.; Sirjean, B.; Battin-Leclerc, F.; Wang, Z.; Xie, M.; Cheng, Z.; Qi, F. *Combust. Flame* **2012**, *159*, 3455.
(3) Yin, H. Y.; Xu, L. B.; Porter, N. A. *Chem. Rev.* **2011**, *111*, 5944.
(4) Gugumus, F. *Polym. Degrad. Stab.* **2006**, *91*, 3416.
(5) (a) Jensen, R. K.; Korcek, S.; Mahoney, L. R.; Zinbo, M. *J. Am. Chem. Soc.* **1979**, *101*, 7574. (b) Jensen, R. K.; Korcek, S.; Mahoney, L. R.; Zinbo, M. *J. Am. Chem. Soc.* **1981**, *103*, 1742. (c) Jensen, R. K.; Korcek, S.; Zinbo, M.; Johnson, M. D. *Int. J. Chem. Kinet.* **1990**, *22*, 1095. (d) Jensen, R. K.; Zinbo, M.; Korcek, S. *J. Chromatogr. Sci.* **1983**, *21*, 394. (e) Blaine, S.; Savage, P. E. *Ind. Eng. Chem. Res.* **1991**, *30*, 792. (f) Blaine, S.; Savage, P. E. *Ind. Eng. Chem. Res.* **1991**, *30*, 2185. (g) Blaine, S.; Savage, P. E. *Ind. Eng. Chem. Res.* **1992**, *31*, 69.
(6) Pfaendtner, J.; Broadbelt, L. J. *Ind. Eng. Chem. Res.* **2008**, *47*, 2886.
(7) Hamilton, E. J.; Korcek, S.; Mahoney, L. R.; Zinbo, M. *Int. J. Chem. Kinet.* **1980**, *12*, 577.
(8) Zador, J.; Taatjes, C. A.; Fernandes, R. X. *Prog. Energy Combust. Sci.* **2011**, *37*, 371.
(9) (a) Cord, M.; Husson, B.; Lizardo Huerta, J. C.; Herbinet, O.; Glaude, P.-A.; Fournet, R.; Sirjean, B.; Battin-Leclerc, F.; Ruiz-Lopez, M.; Wang, Z.; Xie, M.; Cheng, Z.; Qi, F. *J. Phys. Chem. A* **2012**, *116*, 12214. (b) Herbinet, O.; Battin-Leclerc, F.; Bax, S.; Le Gall, H.; Glaude, P. A.; Fournet, R.; Zhou, Z. Y.; Deng, L. L.; Guo, H. J.; Xie, M. F.; Qi, F. *Phys. Chem. Chem. Phys.* **2011**, *13*, 296.
(10) Baumstark, A. L.; Vasquez, P. C. *J. Heterocycl. Chem.* **1992**, *29*, 1781.
(11) Zhao, Y.; Truhlar, D. G. *Theor. Chem. Acc.* **2008**, *120*, 215.
(12) Lynch, B. J.; Zhao, Y.; Truhlar, D. G. *J. Phys. Chem. A* **2003**, *107*, 1384.
(13) (a) Clark, T.; Chandrasekhar, J.; Spitznagel, G. W.; Schleyer, P. V. *J. Comput. Chem.* **1983**, *4*, 294. (b) Frisch, M. J.; Pople, J. A.; Binkley, J. S. *J. Chem. Phys.* **1984**, *80*, 3265.
(14) (a) Alecu, I. M.; Truhlar, D. G. *J. Phys. Chem. A* **2011**, *115*, 2811. (b) Xu, X. F.; Alecu, I. M.; Truhlar, D. G. *J. Chem. Theory Comput.* **2011**, *7*, 1667. (c) Zheng, J.; Truhlar, D. G. *Phys. Chem. Chem. Phys.* **2010**, *12*, 7782. (d) Alecu, I. M.; Truhlar, D. G. *J. Phys. Chem. A* **2011**, *115*, 14599.
(15) Alecu, I. M.; Zheng, J.; Zhao, Y.; Truhlar, D. G. *J. Chem. Theory Comput.* **2010**, *6*, 2872.
(16) Frisch, M. J.; Trucks, G. W.; Schlegel, H. B.; Scuseria, G. E.; Robb, M. A.; Cheeseman, J. R.; Scalmani, G.; Barone, V.; Mennucci, B.; Petersson, G. A.; Nakatsuji, H.; Caricato, M.; Li, X.; Hratchian, H. P.; Izmaylov, A. F.; Bloino, J.; Zheng, G.; Sonnenberg, J. L.; Hada, M.; Ehara, M.; Toyota, K.; Fukuda, R.; Hasegawa, J.; Ishida, M.; Nakajima, T.; Honda, Y.; Kitao, O.; Nakai, H.; Vreven, T.; Montgomery, J. A., Jr.; Peralta, J. E.; Ogliaro, F.; Bearpark, M.; Heyd, J. J.; Brothers, E.; Kudin, K. N.; Staroverov, V. N.; Kobayashi, R.; Normand, J.; Raghavachari, K.; Rendell, A.; Burant, J. C.; Iyengar, S. S.; Tomasi, J.; Cossi, M.; Rega, N.; Millam, J. M.; Klene, M.; Knox, J. E.; Cross, J. B.; Bakken, V.; Adamo, C.; Jaramillo, J.; Gomperts, R.; Stratmann, R. E.; Yazyev, O.; Austin, A. J.; Cammi, R.; Pomelli, C.; Ochterski, J. W.; Martin, R. L.; Morokuma, K.; Zakrzewski, V. G.; Voth, G. A.; Salvador, P.; Dannenberg, J. J.; Dapprich, S.; Daniels, A. D.; Farkas, Ö.; Foresman, J. B.; Ortiz, J. V.; Cioslowsk, J.; Fox, D. J. *Gaussian 09*, revision A.1; Gaussian Inc.; Wallingford, CT; 2009.
(17) (a) Adler, T. B.; Knizia, G.; Werner, H. J. *J. Chem. Phys.* **2007**, *127*, 221106. (b) Adler, T. B.; Werner, H. J.; Manby, F. R. *J. Chem. Phys.* **2009**, *130*, 054106. (c) Knizia, G.; Adler, T. B.; Werner, H. J. *J. Chem. Phys.* **2009**, *130*, 054104.
(18) Werner, H.-J.; Knowles, P. J.; Knizia, G.; Manby, F. R.; Schütz, M.; Celani, P.; Korona, T.; Lindh, R.; Mitrushenkov, A.; Rauhut, G.; Shamasundar, K. R.; Adler, T. B.; Amos, R. D.; Bernhardsson, A.; Berning, A.; Cooper, D. L.; Deegan, M. J. O.; Dobbyn, A. J.; Eckert, F.; Goll, E.; Hampel, C.; Hesselmann, A.; Hetzer, G.; Hrenar, T.; Jansen, G.; Köppl, C.; Liu, Y.; Lloyd, A. W.; Mata, R. A.; May, A. J.; McNicholas, S. J.; Meyer, W.; Mura, M. E.; Nicklass, A.; O'Neill, D. P.; Palmieri, P.; Pflüger, K.; Pitzer, R.; Reiher, M.; Shiozaki, T.; Stoll, H.; Stone, A. J.; Tarroni, R.; Thorsteinsson, T.; Wang, M.; Wolf, A. *Molpro*, v2010.1.; University College Cardiff Consultants Limited: Cardiff, U.K., 2010; http://www.molpro.net.
(19) (a) Bartlett, R. J.; Musial, M. *Rev. Mod. Phys.* **2007**, *79*, 291. (b) Raghavachari, K.; Trucks, G. W.; Pople, J. A.; Headgordon, M. *Chem. Phys. Lett.* **1989**, *157*, 479.
(20) (a) Klopper, W.; Noga, J. In *Explicitly Correlated Wave Functions in Chemistry and Physics*; Rychlewski, J., Ed.; Kluwer: Dordrecht, 2003. (b) Noga, J.; Kutzelnigg, W. *J. Chem. Phys.* **1994**, *101*, 7738.
(21) (a) Aguilera-Iparraguirre, J.; Curran, H. J.; Klopper, W.; Simmie, J. M. *J. Phys. Chem. A* **2008**, *112*, 7047. (b) Seal, P.; Papajak, E.; Yu, T.; Truhlar, D. G. *J. Chem. Phys.* **2012**, *136*, 034306. (c) Seal, P.; Papajak, E.; Truhlar, D. G. *J. Phys. Chem. Lett.* **2012**, *3*, 264. (d) Alecu, I. M.; Zheng, J.; Papajak, E.; Yu, T.; Truhlar, D. G. *J. Phys. Chem. A* **2012**, *116*, 12206. (e) Seal, P.; Oyedepo, G.; Truhlar, D. G. *J. Phys. Chem. A* **2013**, *117*, 275. (f) Zheng, J.; Seal, P.; Truhlar, D. G. *Chem. Sci* **2013**, *4*, 200. (g) Papajak, E.; Seal, P.; Xu, X.; Truhlar, D. G. *J. Chem. Phys.* **2012**, 137.
(22) Zheng, J.; Zhao, Y.; Truhlar, D. G. *J. Phys. Chem. A* **2007**, *111*, 4632.
(23) Peterson, K. A.; Adler, T. B.; Werner, H. J. *J. Chem. Phys.* **2008**, 128.
(24) (a) Yu, T.; Zheng, J.; Truhlar, D. G. *J. Phys. Chem. A* **2012**, *116*, 297. (b) Zheng, J.; Truhlar, D. G. *Faraday Discuss.* **2012**, *157*, 59.
(25) (a) Liu, Y. P.; Lynch, G. C.; Truong, T. N.; Lu, D. H.; Truhlar, D. G.; Garrett, B. C. *J. Am. Chem. Soc.* **1993**, *115*, 2408. (b) Fernandez-Ramos, A.; Ellingson, B. A.; Garrett, B. C.; Truhlar, D. G. In *Reviews in Computational Chemistry*; Lipkowitz, K. B., Cundari, T. R., Eds.; Wiley-VCH: Hoboken, NJ, 2007; Vol. 23, p 125.
(26) Yu, T.; Zheng, J.; Truhlar, D. G. *Chem. Sci* **2011**, *2*, 2199.
(27) (a) Zheng, J.; Mielke, S. L.; Clarkson, K. L.; Truhlar, D. G. *Comput. Phys. Commun.* **2012**, *183*, 1803. (b) Zheng, J. J.; Yu, T.; Papajak, E.; Alecu, I. M.; Mielke, S. L.; Truhlar, D. G. *Phys. Chem. Chem. Phys.* **2011**, *13*, 10885.
(28) (a) Yu, T.; Zheng, J.; Truhlar, D. G. *Phys. Chem. Chem. Phys.* **2012**, *14*, 482. (b) Zheng, J.; Yu, T.; Truhlar, D. G. *Phys. Chem. Chem. Phys.* **2011**, *13*, 19318.
(29) (a) Pollak, E.; Pechukas, P. *J. Am. Chem. Soc.* **1978**, *100*, 2984. (b) Fernandez-Ramos, A.; Ellingson, B. A.; Meana-Pañeda, R.; Marques, J. M. C.; Truhlar, D. G. *Theor. Chem. Acc.* **2007**, *118*, 813.
(30) (a) Marcus, R. A.; Coltrin, M. E. *J. Chem. Phys.* **1977**, *67*, 2609. (b) Bondi, D. K.; Connor, J. N. L.; Garrett, B. C.; Truhlar, D. G. *J. Chem. Phys.* **1983**, *78*, 5981. (c) Kreevoy, M. M.; Ostovic, D.; Truhlar, D. G.; Garrett, B. C. *J. Phys. Chem.* **1986**, *90*, 3766. (d) Liu, Y. P.; Lu, D. H.; Gonzalez-Lafont, A.; Truhlar, D. G.; Garrett, B. C. *J. Am. Chem. Soc.* **1993**, *115*, 7806. (e) Fernandez-Ramos, A.; Truhlar, D. G. *J. Chem. Phys.* **2001**, *114*, 1491. (f) Garrett, B. C.; Truhlar, D. G. *J. Chem. Phys.* **1983**, *79*, 4931. (g) Meana-Pañeda, R.; Truhlar, D. G.; Fernandez-Ramos, A. *J. Chem. Theory Comput.* **2010**, *6*, 6.
(31) (a) Garrett, B. C.; Truhlar, D. G.; Grev, R. S.; Magnuson, A. W. *J. Phys. Chem.* **1980**, *84*, 1730. (b) Truhlar, D. G.; Garrett, B. C. *Acc. Chem. Res.* **1980**, *13*, 440.
(32) Zheng, J.; Zhang, S.; Lynch, B. J.; Corchado, J. C.; Chuang, Y.-Y.; Fast, P. L.; Hu, W.-P.; Liu, Y.-P.; Lynch, G. C.; Nguyen, K. A.;

Jackels, C. F.; Ramos, A. F.; Ellingson, B. A.; Melissas, V. S.; Villa, J.; Rossi, I.; Coitiño, E. L.; Pu, J.; Albu, T. V.; Steckler, R.; Garrett, B. C.; Isaacson, A. D.; Truhlar, D. G. *POLYRATE*, v.2010-A; University of Minnesota: Minneapolis, MN, 2010.
(33) Zheng, J.; Zhang, S.; Corchado, J. C.; Chuang, Y.-Y.; Coitiño, E. L.; Ellingson, B. A.; Truhlar, D. G. *GAUSSRATE*, v.2009-A.; University of Minnesota: Minneapolis, MN, 2009.
(34) Chuang, Y. Y.; Truhlar, D. G. *J. Phys. Chem. A* **1998**, *102*, 242.
(35) Melissas, V. S.; Truhlar, D. G.; Garrett, B. C. *J. Chem. Phys.* **1992**, *96*, 5758.
(36) Page, M.; McIver, J. W. *J. Chem. Phys.* **1988**, *88*, 922.
(37) Villa, J.; Truhlar, D. G. *Theor. Chem. Acc.* **1997**, *97*, 317.
(38) (a) Natanson, G. A.; Garrett, B. C.; Truong, T. N.; Joseph, T.; Truhlar, D. G. *J. Chem. Phys.* **1991**, *94*, 7875. (b) Jackels, C. F.; Gu, Z.; Truhlar, D. G. *J. Chem. Phys.* **1995**, *102*, 3188.
(39) Ernzerhof, M.; Perdew, J. P. *J. Chem. Phys.* **1998**, *109*, 3313.
(40) Goldsmith, C. F.; Green, W. H.; Klippenstein, S. J. *J. Phys. Chem. A* **2012**, *116*, 3325.
(41) (a) Cramer, C. J.; Truhlar, D. G. *Chem. Rev.* **1999**, *99*, 2161. (b) Ashcraft, R. W.; Raman, S.; Green, W. H. *J. Phys. Chem. B* **2007**, *111*, 11968. (c) Jalan, A.; Ashcraft, R. W.; West, R. H.; Green, W. H. *Annu. Rep. Prog. Chem., Sect. C: Phys. Chem.* **2010**, *106*, 211−258. (d) Jalan, A.; West, R. H.; Green, W. H. *J. Phys. Chem. B* **2013**, *117*, 2955. (e) Chuang, Y. Y.; Cramer, C. J.; Truhlar, D. G. *Int. J. Quantum Chem.* **1998**, *70*, 887.
(42) Ben-Naim, A. *Solvation Thermodynamics*; Plenum: New York, 1987.
(43) Cances, E.; Mennucci, B.; Tomasi, J. *J. Chem. Phys.* **1997**, *107*, 3032.
(44) Tomasi, J.; Mennucci, B.; Cammi, R. *Chem. Rev.* **2005**, *105*, 2999.
(45) Marenich, A. V.; Cramer, C. J.; Truhlar, D. G. *J. Phys. Chem. B* **2009**, *113*, 6378.
(46) Ho, J. M.; Klamt, A.; Coote, M. L. *J. Phys. Chem. A* **2010**, *114*, 13442.
(47) Cramer, C. J.; Truhlar, D. G. *Acc. Chem. Res.* **2008**, *41*, 760.
(48) da Silva, G. *Angew. Chem., Int. Ed.* **2010**, *49*, 7523.
(49) Pfaendtner, J.; Broadbelt, L. J. *Ind. Eng. Chem. Res.* **2008**, *47*, 2897.
(50) Andrews, D. U.; Heazlewood, B. R.; Maccarone, A. T.; Conroy, T.; Payne, R. J.; Jordan, M. J. T.; Kable, S. H. *Science* **2012**, *337*, 1203.
(51) Archibald, A. T.; McGillen, M. R.; Taatjes, C. A.; Percival, C. J.; Shallcross, D. E. *Geophys. Res. Lett.* **2007**, *34*, L21801.
(52) Taatjes, C. A.; Hansen, N.; McIlroy, A.; Miller, J. A.; Senosiain, J. P.; Klippenstein, S. J.; Qi, F.; Sheng, L. S.; Zhang, Y. W.; Cool, T. A.; Wang, J.; Westmoreland, P. R.; Law, M. E.; Kasper, T.; Kohse-Hoinghaus, K. *Science* **2005**, *308*, 1887.
(53) (a) Taatjes, C. A.; Welz, O.; Eskola, A. J.; Savee, J. D.; Osborn, D. L.; Lee, E. P. F.; Dyke, J. M.; Mok, D. W. K.; Shallcross, D. E.; Percival, C. J. *Phys. Chem. Chem. Phys.* **2012**, *14*, 10391. (b) Welz, O.; Savee, J. D.; Osborn, D. L.; Vasu, S. S.; Percival, C. J.; Shallcross, D. E.; Taatjes, C. A. *Science* **2012**, *335*, 204.
(54) Tishchenko, O.; Ilieva, S.; Truhlar, D. G. *J. Chem. Phys.* **2010**, *133*, 02110.
(55) *CanTherm*, v2013; https://github.com/GreenGroup/RMG-Py (accessed June 15, 2013).
(56) Green, N. J. B.; Bhatti, Z. A. *Phys. Chem. Chem. Phys.* **2007**, *9*, 4275.
(57) Joback, K. G. A Unified Approach to Physical Property Estimation using Multivariate Statistical Techniques. M.S. Thesis, *Massachusetts Institute of Technology*, June 1984.
(58) Jasper, A. W.; Miller, J. A. *J. Phys. Chem. A* **2011**, *115*, 6438.
(59) Carstensen, H.-H.; Dean, A. M. In *Comprehensive Chemical Kinetics*; Robert, W. C., Ed.; Elsevier: Amsterdam, 2007; Vol. *42*, p 101.
(60) Yee, L. D.; Craven, J. S.; Loza, C. L.; Schilling, K. A.; Ng, N. L.; Canagaratna, M. R.; Ziemann, P. J.; Flagan, R. C.; Seinfeld, J. H. *J. Phys. Chem. A* **2012**, *116*, 6211.
(61) Sarathy, S. M.; Vranckx, S.; Yasunaga, K.; Mehl, M.; Oßwald, P.; Metcalfe, W. K.; Westbrook, C. K.; Pitz, W. J.; Kohse-Höinghaus, K.; Fernandes, R. X.; Curran, H. J. *Combust. Flame* **2012**, *159*, 2028.
(62) (a) Jahn, U.; Galano, J. M.; Durand, T. *Angew. Chem., Int. Ed.* **2008**, *47*, 5894. (b) Frankel, E. N. *J. Am. Oil Chem. Soc.* **1984**, *61*, 1908.
(63) Porter, N. A.; Funk, M. O.; Gilmore, D.; Isaac, R.; Nixon, J. *J. Am. Chem. Soc.* **1976**, *98*, 6000.